Landscape response to Pleistocene-Holocene precipitation change in the Western Cordillera, Peru: ^{10}Be concentrations in modern sediments and terrace fills

Devin McPhillips,[1] Paul R. Bierman,[1] Thomas Crocker,[2] and Dylan H. Rood[3,4]

Received 25 April 2013; revised 19 October 2013; accepted 25 October 2013; published 12 December 2013.

[1] The landscape response to climate change is frequently investigated with models because natural experiments on geologic timescales are rare. In Quebrada Veladera, in the western Andes Mountains, the formation of alluvial terraces during periods of high precipitation presents opportunities for such an experiment. We compare drainage-average erosion rates during Pleistocene terrace deposition with Holocene rates, using cosmogenic ^{10}Be samples for seven pairs of quartz sand taken from the trunk and tributaries of Quebrada Veladera and adjacent terraces. Each pair consists of sediment collected from the modern channel and excavated from an adjacent fill terrace. The terrace fill was deposited at ~16 ka and preserved an isotopic record of paleoerosion rates in the Late Pleistocene. Modern sands yield ^{10}Be concentrations between 1.68×10^5 and 2.28×10^5 atoms/g, corresponding to Holocene erosion rates between 43 ± 3 and 58 ± 4 mm/kyr. The ^{10}Be concentrations in terrace sands range from 9.46×10^4 to 3.73×10^5 atoms/g, corresponding to paleoerosion rates from 27 ± 2 to 103 ± 8 mm/kyr. Smaller, upstream tributaries show a substantial decline in erosion rate following the transition from a wet to dry climate, but larger drainage areas show no change. We interpret this trend to indicate that the wetter climate drove landscape dissection, which ceased with the return to dry conditions. As channel heads propagated upslope, erosion accelerated in low-order drainages before higher-order ones. This contrast disappeared when the drainage network ceased to expand; at that point, erosion rates became spatially uniform, consistent with the uniformity of modern hillslope gradients.

Citation: McPhillips, D., P. R. Bierman, T. Crocker, and D. H. Rood (2013), Landscape response to Pleistocene-Holocene precipitation change in the Western Cordillera, Peru: ^{10}Be concentrations in modern sediments and terrace fills, *J. Geophys. Res. Earth Surf.*, *118*, 2488–2499, doi:10.1002/2013JF002837.

1. Introduction

[2] The response of landscapes to Quaternary climate change is a fundamental concern of geomorphology [*National Research Council*, 2010]. In regions such as coastal Peru, Quaternary sedimentary deposits are often interpreted as proxies for Pleistocene-Holocene climate change or variability in El Niño–Southern Oscillation (ENSO) [*Sandweiss et al.*, 2001; *Keefer et al.*, 2003; *Ortlieb and Vargas*, 2003; *Sandweiss*, 2003; *Trauth et al.*, 2003; *Steffen et al.*, 2009, 2010]. Many climatic interpretations rely on concepts developed in modern landscapes because landscape responses are difficult to determine on geologic timescales [*Harvey*, 2005; *Dorn*, 2009; *Enzel et al.*, 2012]. Recently, work has begun to address this limitation by establishing chronologies for detailed stratigraphic relationships among terrace fills, alluvial fans, and soils [*Anders et al.*, 2005; *Harvey and Pederson*, 2011; *Enzel et al.*, 2012]. In this study, we take a different approach and use cosmogenic ^{10}Be to compare Pleistocene and Holocene drainage-scale erosion rates. Our aim is to measure the landscape response to climate change, especially in terms of landscape dissection and annealing.

[3] Concentrations of ^{10}Be and other cosmogenic radionuclides are often interpreted in terms of drainage average erosion rates [*Brown et al.*, 1995; *Bierman and Steig*, 1996; *Granger et al.*, 1996; *Von Blanckenburg*, 2005] or rates of transport or mixing [*Bierman and Nichols*, 2004]. Pleistocene-Holocene changes in erosion rates are detected by measuring cosmogenic isotope concentrations in sedimentary archives, such as deposits of fluvial sediment [*Schaller et al.*, 2002; *Schaller and Ehlers*, 2006; *Fuller et al.*, 2009; *Wittmann et al.*, 2011a; *Davis et al.*, 2012]. For example, *Schaller et al.* [2002] used ^{10}Be to show that erosion rates from modern sediments of the Meuse River,

Additional supporting information may be found in the online version of this article.

[1]Department of Geology, University of Vermont, Burlington, Vermont, USA.
[2]Department of Geology, Middlebury College, Middlebury, Vermount, USA.
[3]AMS Laboratory, Scottish Universities Environmental Research Centre, Scotland, UK.
[4]Earth Research Institute, University of California, Santa Barbara, California, USA.

Corresponding author: D. McPhillips, Department of Geology, University of Vermont, 180 Colchester Ave. Burlington, VT 05405, USA. (devin.mcphillips@gmail.com)

2169-9003/13/10.1002/2013JF002837

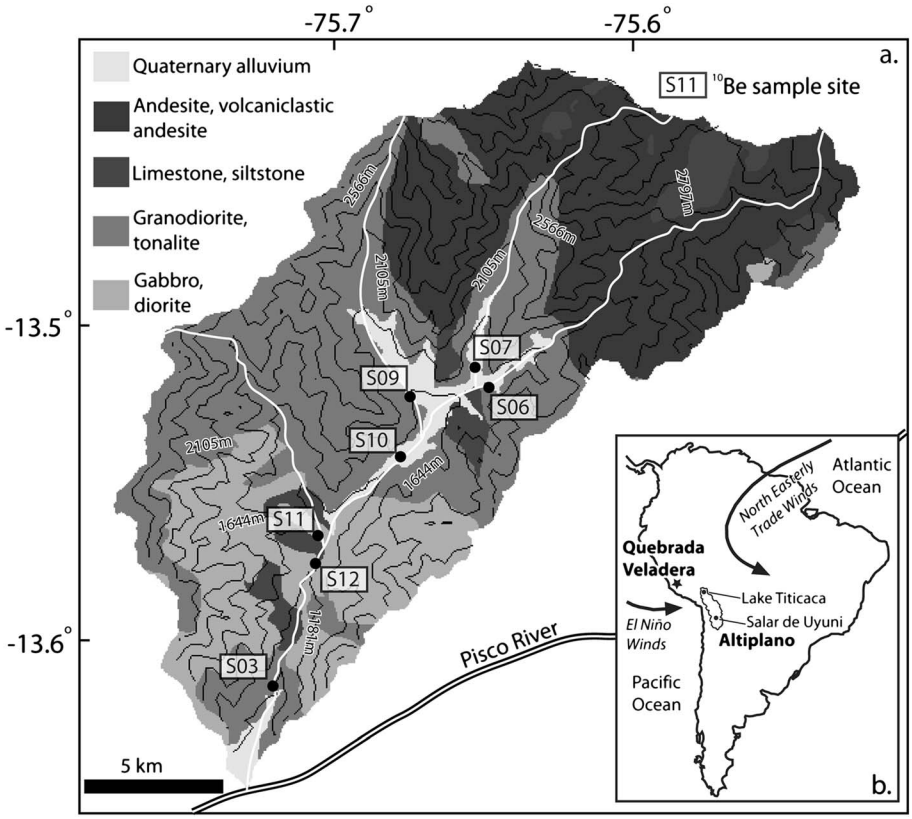

Figure 1. (a) Geologic map of Quebrada Veladera. ^{10}Be sample sites are shown as black circles with the labels used in Table 2. The stream channels are traced in white. Only the drainage area with quartz-bearing bedrock (granodiorite and tonalite) was used to calculate ^{10}Be production rates. (b) Location map positioning Quebrada Veladera relative to South America and predominant sources of winds and moisture. Lake Titicaca and Salar de Uyuni are sites with records of Quaternary paleolake levels. The boundary of the Altiplano is defined here by its internal drainage basin. (Geologic map modified from *Diaz and Landa* [1970] and *Davila* [1979]. Location map modified from *Placzek et al*. [2006]).

in northern Europe, are 50% lower than paleoerosion rates from nearby alluvial terraces. They interpreted this change to reflect the decline of periglacial processes following the Last Glacial Maximum. Even in drainages with large floodplains, such as the Amazon, most ^{10}Be is produced on the hillslopes, either in regolith or near-surface bedrock, rather than during transport by streams [e.g., *Heimsath et al*., 1997, 1999; *Wittmann and Von Blanckenburg*, 2009]. The burial of sedimentary archives often preserves the ^{10}Be concentration inherited from the hillslopes by limiting in situ cosmogenic production [*Cox et al*., 2009].

[4] Large drainages may mask the landscape response to changes in climate or land use because of buffering from sediment storage or because the changes are not uniform over the drainage area [*Graf*, 1987; *Anders et al*., 2005]. For example, at the outlets of the Amazon and the Nile Rivers, the absence of a detectable glacial-interglacial change in ^{10}Be concentration has been attributed to buffering by reworking of ancient sediment in floodplains [*Wittmann et al*., 2011a; *Davis et al*., 2012]. Very small drainages are problematic for the opposite reason: There is not enough capacity for sediment mixing to average the effects of large, stochastic events such as landslides [*Niemi et al*., 2005; *Yanites et al*., 2009]. As a result, the most clear-cut results regarding the geomorphic controls on landscape response are likely to come from studies that focus on moderately sized, upland drainages.

[5] Here we present a detailed cosmogenic nuclide investigation of a mountainous drainage in the northwestern foothills of the Andean Altiplano. This drainage, Quebrada Veladera, is a tributary of the Pisco River. *Steffen et al*. [2009] dated alluvial terraces along the Pisco using infrared stimulated luminescence (IRSL). We correlate two of the Pisco terraces with contiguous terraces in Quebrada Veladera. The correlation indicates that the lower terrace fill in Quebrada Veladera was deposited at ~16 ka, synchronous with a paleolake highstand on the Altiplano [*Placzek et al*., 2006]. We report ^{10}Be concentrations in paired sand samples collected from the 16 ka terrace fill as well as the modern channel of the trunk stream and its tributaries. We use these data to directly compare erosion rates under the contemporary climate with Late Pleistocene rates. At the latitude and elevation of Quebrada Veladera (~13.7°S, 900 to 3900 m), the Late Pleistocene climate was wetter than it is today but still too warm to support glacial ice [*Klein et al*., 1999; *Ramage et al*., 2005; *Smith et al*., 2005]. We examine the spatial and temporal variability of erosion rates in order to assess landscape-scale geomorphic process. We also address the implications of landscape response for the Late Pleistocene climate.

Table 1. Chronology of Pisco River Terraces and Paleolake Highstands

Terrace Name	Terrace Age[a] (ka)	Highstand Name	Highstand Age (ka)
T1	54 to 38	Minchin[b]	50 to 41
T2	24 to 16	Tauca[c]	25 to 11
T3	11 to 4	-	-

[a]Range of infrared-stimulated luminescence ages reported by *Steffen et al*. [2009].

[b]We follow the naming convention of *Steffen et al*. [2009]. Recent work favors a shorter, smaller highstand named Inca Huasi (45 to 47 ka) [*Placzek et al*., 2006].

[c]Again, we follow *Steffen et al*. [2009]. *Placzek et al*. [2006] divide the Tauca into the Sajsi (24 to 20 ka), the Tauca proper (18 to 14 ka), and the Coipasa (13 to 11 ka).

2. Background

2.1. Geologic Setting

[6] The field site for this study, Quebrada Veladera, is a moderately sized (315 km^2) tributary of the Pisco River. The Pisco drains an area from the northern edge of the Andean Altiplano to the Pacific Coast (Figure 1). Alluvial terraces are preserved along its banks between the Pacific coast and a knickzone at about 3 km elevation, 80 km inland [*Steffen et al*., 2009]. Three terrace levels are present along the Pisco: T1, T2, and T3. IRSL dates from these terraces suggest that the two largest formed in the late Quaternary, coincident with periods of high water in Altiplano paleolakes: the Tauca and Minchin/Inca Huasi lake cycle highstands. *Steffen et al*. [2009] interpreted the timing to indicate that the terraces formed in response to an increase in the amount and intensity of precipitation, as suggested by modeling [e.g., *Tucker and Slingerland*, 1997]. In this view, enhanced precipitation increased transport capacity in the drainage during the paleolake highstands [e.g., *Placzek et al*., 2006], thereby shifting sediment from hillslopes into fill deposits along the trunk stream. Planation and incision, forming the terraces, began as the hillslope sediment supply was exhausted but before the climate reverted to the modern, arid state. At the precision of the IRSL dates, the deposition of terrace fills was contemporaneous with paleolake highstands (Table 1).

[7] Quebrada Veladera joins the Pisco in the Andean foothills, 55 km from the coast, and just downstream from an IRSL sampling site [*Steffen et al*., 2009] (Figure 1). The quebrada contains two alluvial terraces, which we correlate with the Pisco River terraces T1 and T2 based on height and stratigraphy. Large, trenched alluvial fans may be the local expression of the T3 terrace fill [e.g., *Rigsby et al*., 2003; *Steffen et al*., 2010]. In the quebrada, we term the higher terrace Q1 and the lower terrace Q2. This reflects the numbering of the Pisco River terraces by *Steffen et al*. [2009]. IRSL dates link Q1 and T1 (54 to 38 ka) with the Minchin/Inca Huasi paleolake highstand and Q2 and T2 (24 to 16 ka) with the Tauca highstand(s). T3 is younger, dated at 11 to 4 ka.

[8] It is possible to walk along the T2 terrace surface above the Pisco River channel directly onto the Q2 surface in Quebrada Veladera, interrupted only briefly by highway fill material. At the mouth of the quebrada, the T2 surface transitions into Q2 at a constant height of ~8 m above both channels. The Q2 terrace continues upstream for more than 20 km as a nearly continuous surface that is usually paired across the stream channel (Figure 2). The sediment fill below the Q2 surface is characterized by thickly bedded, clast-supported conglomerates, and massive silty sands (Figure 3). Diamicts are also common, especially in association with tributary confluences and alluvial fans. These strata are typically matrix supported, with angular to subangular clasts and monomict lithologies, but they show substantial variability. The base of the Q2 fill is frequently in direct contact with bedrock.

[9] The T1 terrace stands more than 50 m above the Pisco River and appears to transition into the Q1 terrace at a similar height in Quebrada Veladera. However, Q1 is discontinuous within the quebrada. It frequently exists only as a thin strip of conglomerate or diamict hanging on the valley wall, 30 m or more above the channel. Diamicts appear more common in the Q1 terrace fills than below the Q2 level, but the comparison is uncertain due to limited exposure.

[10] The terrace stratigraphy in Quebrada Veladera agrees closely with the description of Pisco River terrace fills [*Steffen et al*., 2009]. We interpret conglomerate beds as recording perennial flow in a braided stream. Imbricated cobble beds probably represent longitudinal bars, while silty sands record slackwater deposition following flood peaks [*Miall*, 1996]. Limited sorting and subangular to subrounded clasts suggest that transport took place over short distances and at high velocities. Nonetheless, polymict lithogies are representative of upstream bedrock and indicate substantial mixing during transport. Diamicts record locally sourced mass movements [*Costa*, 1988] and debris flow deposits. We interpret their variability to primarily reflect differences in the sediment concentration and transport distance of individual events.

[11] Terrace fill deposition probably occurred continuously, at least at the outcrop scale. This is evidenced by the absence of large-scale scours or paleosols anywhere in the section to indicate extended depositional hiatuses. Shallow debris flows appear to contribute substantially to the modern sediment load (Figure 3) and were probably important during fill terrace deposition as well [*Mettier et al*., 2009; *Steffen et al*., 2009, 2010]. Without a detailed chronology of the stratigraphy, it is difficult to correlate individual depositional events along the length of the terrace. The absence of organic matter in the fill deposits precludes a ^{14}C chronology. The overall fining upward in the Q2 fill may indicate that terrace

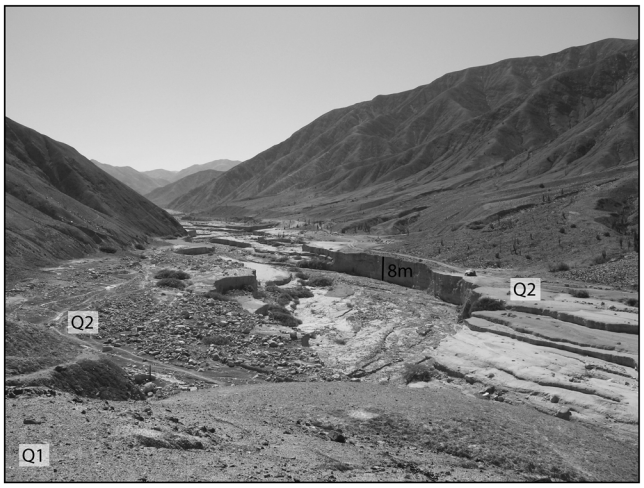

Figure 2. Photo looking north, taken downstream from sample site S11. The Q1 and Q2 terraces are labeled.

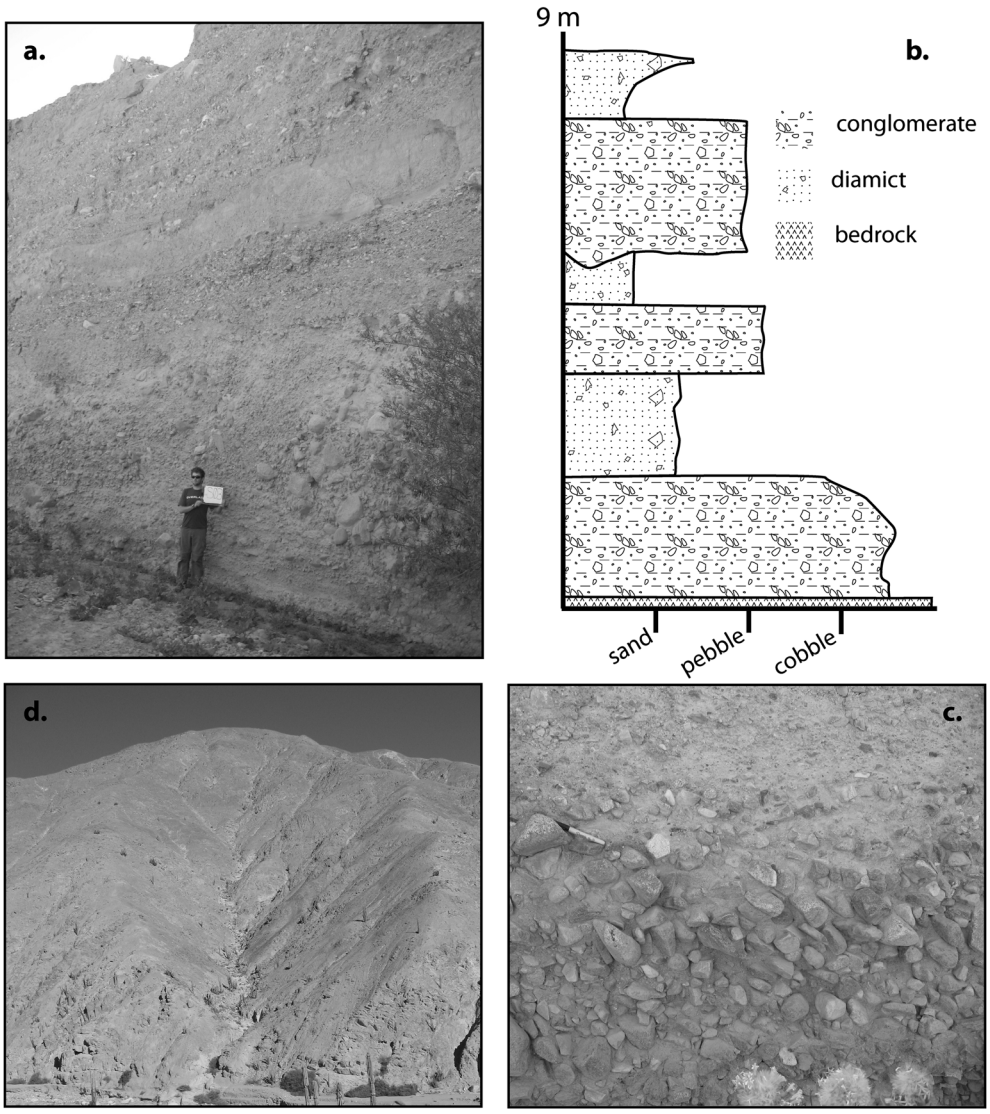

Figure 3. Character of the Q2 terrace. (a) Photo of the Q2 terrace at site S03. (b) Stratigraphic log at S03, which is representative of the Q2 terrace. (c) Detail of imbricated clasts. (d) A small, modern tributary (~1 km^2) characterized by shallow debris flow channels.

incision followed a decline in sediment supply from the hillslopes of the drainage (Figure 3).

[12] Modern streams in our field area are dry for most of the year and appear to be transport limited. The channels contain longitudinal bars that are characterized by subangular to subrounded cobbles and boulders. The lithologies are diverse and representative of upstream bedrock. Although the channels are typically in sediment, bedrock is regularly exposed throughout the drainage network.

[13] The majority of the bedrock in Quebrada Veladera is Coastal Batholith, primarily quartz-bearing granodiorite and tonalite that crystallized in the Cretaceous [*Diaz and Landa*, 1970; *Davila*, 1979]. The headwaters contain substantial amounts of Upper Cretaceous and Tertiary cover rocks, including limestone, shale, and andesite (Figure 1). Andesite hand samples and thin sections contain a few percent or less quartz, while the crystalline batholith contains 20% or more. The batholith is therefore the dominant source of sand-size quartz in stream sediment.

2.2. Climatic Setting

[14] The present climate is extremely dry in Quebrada Veladera. Vegetation is limited to sparse cacti at higher elevations and brush along the wetter channel reaches. Precipitation averages less than 200 mm/yr in this region and decreases to near zero at the coast [*Agteca*, 2010]. Along the coast, however, precipitation amounts have substantial interannual variability. In typical years, easterly winds deliver moisture from the Amazon Basin, but in strong El Niño years, westerly winds from the Pacific deliver substantially more precipitation to the coast [*Mettier et al*., 2009]. These westerly winds also inhibit moisture transport from the Amazon, leading to dryness on the Altiplano [*Garreaud et al*., 2003].

[15] In the past, the climate was occasionally wetter. Drill cores and paleoshorelines on the Altiplano show at least two major transgressions of lakes and salars since 140 ka [*Thompson et al*., 1998; *Baker et al*., 2001a, 2001b; *Thompson et al*., 2003; *Fritz et al*., 2004; *Placzek et al*., 2006]. Trangressions and highstands are widely interpreted

as periods of increased precipitation, with the caveat that lake levels are a function of basin geometry as well as precipitation. The ^{14}C and U-Th dates give consistent chronologies, indicating that the Altiplano was relatively wet from about 25 to 11 ka, which is a period generally termed the Tauca lake cycle [e.g., *Baker et al*., 2001b; *Placzek et al*., 2006]. Depending on the proxy and the dating method, the Tauca may have consisted of a single highstand [e.g., *Baker et al*., 2001b] or three shorter cycles, termed Sajsi, Tauca, and Coipasa [*Placzek et al*., 2006]. Here we simply refer to the Tauca highstand. Several paleolake cycles occurred prior to this event. A widely recognized highstand from 50 to 41 ka is termed either Minchin [e.g., *Baker et al*., 2001b; *Fritz et al*., 2004] or Inca Huasi [*Placzek et al*., 2006]. Gamma radiation logs from lake sediment cores suggest that this lake cycle was at least as deep as Tauca, but paleoshorelines suggest a smaller and briefer transgression. The causes of Altiplano paleolake cycles remain a matter of dispute [e.g., *Placzek et al*., 2006]. Enhanced moisture delivery from the Amazon Basin may have been driven by changes in summer insolation, Pacific sea surface temperature, or other factors [*Garreaud et al*., 2003; *Wang et al*., 2004; *Garreaud et al*., 2009]. Regardless of the cause, it is likely that easterly winds brought additional moisture to the Western Cordillera as well as to the Altiplano [*Garreaud et al*., 2003].

[16] The strength of ENSO during the Quaternary remains a matter of debate. ENSO is relevant because El Niño events in historic time bring large storms and anomalously high amounts of precipitation to the coast of Peru [*Mettier et al*., 2009]. The correlation between historic El Niño events and enhanced coastal precipitation is strongest in northern Peru. Near Quebrada Veladera, the correlation is weaker or even reversed, and El Niño events are correlated with aridity for much of the year [*Lagos et al*., 2008]. Several studies suggest that the effects of El Niño on storms and precipitation were probably weaker than today until at least 5 ka [*Rollins et al*., 1986; *Rodbell et al*., 1999; *Moy et al*., 2002]. Others suggest that ENSO variability had a strong effect in the Early Holocene [*Keefer et al*., 2003; *Rein et al*., 2005; *Makou et al*., 2010]. It is also possible that Early Holocene precipitation variability was present but was driven by atmospheric fluctuations other than ENSO [*Rodbell*, 1992; *Vargas*, 2006].

3. Methods

3.1. Field Methods

[17] We collected paired sediment samples at seven localities within Quebrada Veladera for in situ cosmogenic ^{10}Be analyses. Samples were taken within the four largest tributaries in the quebrada and at three sites along the trunk valley (Figure 1). Each sampling site had a clear expression of the lower terrace, Q2, which we correlate with the Tauca lake cycle (Table 1). Modern sediment samples were collected from the thalweg of the channel, which flows only intermittently. The terrace samples were collected from pits dug >50 cm into the base of the lower terrace at locations that showed evidence of paleostream flow, including rounded and imbricated clasts. In order to ensure that the samples were well mixed and representative of the upstream drainage area, we avoided sampling near alluvial fans and debris flow deposits, which were usually deposited locally. We sieved samples in the field and retained the 250 to 850 μm size fraction. We identified the lithology of clasts and bedrock in hand samples and confirmed field identifications with representative thin sections.

3.2. Stream Morphology

[18] Before evaluating erosion rate changes in response to climate forcing, we first constrained the potential for transient features in the stream system. Transients might result from changes in base level [*Abbühl et al*., 2011] or climate [*Abbühl et al*., 2010] and could complicate the interpretation of spatially variable erosion rates. We identified knickzones using longitudinal channel profiles and slope-area plots. Plots were built from 30 m resolution Advanced Spaceborne Thermal Emission and Reflection Radiometer data [*National Aeronautics and Space Administration (NASA)*, 2006] using the extraction methods of *Wobus et al*. [2006].

3.3. Laboratory Methods

[19] Quartz was purified from sediment samples using standard methods [*Kohl and Nishiizumi*, 1992]. Following magnetic separation, sediments were ultrasonically etched: twice in heated 6 N HCL, 3 times in heated 1% HF-HNO_3, and once in heated 0.5% HF-HNO_3. Any purified quartz sample that contained more than about 150 ppm Al was etched again in 0.5% HF-HNO_3.

[20] Beryllium was extracted from quartz at the University of Vermont Cosmogenic Laboratory. The ^{10}Be was extracted from 18 to 22 g of purified quartz, after the addition of approximately 250 μg of ^{9}Be carrier made from beryl and calibrated to SPEX 1000 ppm standard. One process blank was included for every 11 samples. Following dissolution in hot HF, Be and Al were separated by ion-exchange chromatography, precipitated as hydroxide gels, and finally ignited to form oxides [*Corbett et al*., 2011].

[21] Accelerator mass spectrometer (AMS) measurements were made at Scottish Universities Environmental Research Centre [*Xu et al*., 2010], using a 1:1 mixture of BeO and Nb metal packed in copper cathodes. All standards were normalized to NIST standard material with a reported $^{10}Be/^{9}Be$ ratio of 2.79×10^{-11} and a ^{10}Be half-life of 1.387 Myr [*Nishiizumi et al*., 2007; *Chmeleff et al*., 2010]. Process blank ratios averaged $2.84 \times 10^{-16} \pm 7.91 \times 10^{-17}$ for two measurements, amounting to 0.003 to 0.43% of the sample ratios. The background ratio, at the level of the mean process blank, was subtracted from each sample ratio before calculating concentrations with propagated uncertainties.

3.4. Erosion Rate Calculation

[22] Model erosion rates were calculated using the CRONUS-Earth ^{10}Be–^{26}Al Erosion Rate Calculator Version 2.2.1 [*Balco et al*., 2008]. The calculation employed a constant production rate model and the scaling scheme for spallation of *Lal* [1991] and *Stone* [2000], assuming rock density of 2.75 g/cm^3 and standard atmosphere. Version 2.2.1 of the CRONUS calculator uses a reference spallogenic ^{10}Be production rate of 4.49 ± 0.39 atoms $g^{-1}\,yr^{-1}$ ($\pm 1\sigma$, sea level, high latitude (SLHL)) and muonogenic production after *Heisinger et al*. [2002a, 2002b]. Our results and interpretation are not sensitive to our choice of scaling method (maximum of 11% difference), particularly because our interpretation is primarily based on internal comparison among our samples, and different scaling schemes shift these values systematically. For each sample entered into CRONUS, we first calculated

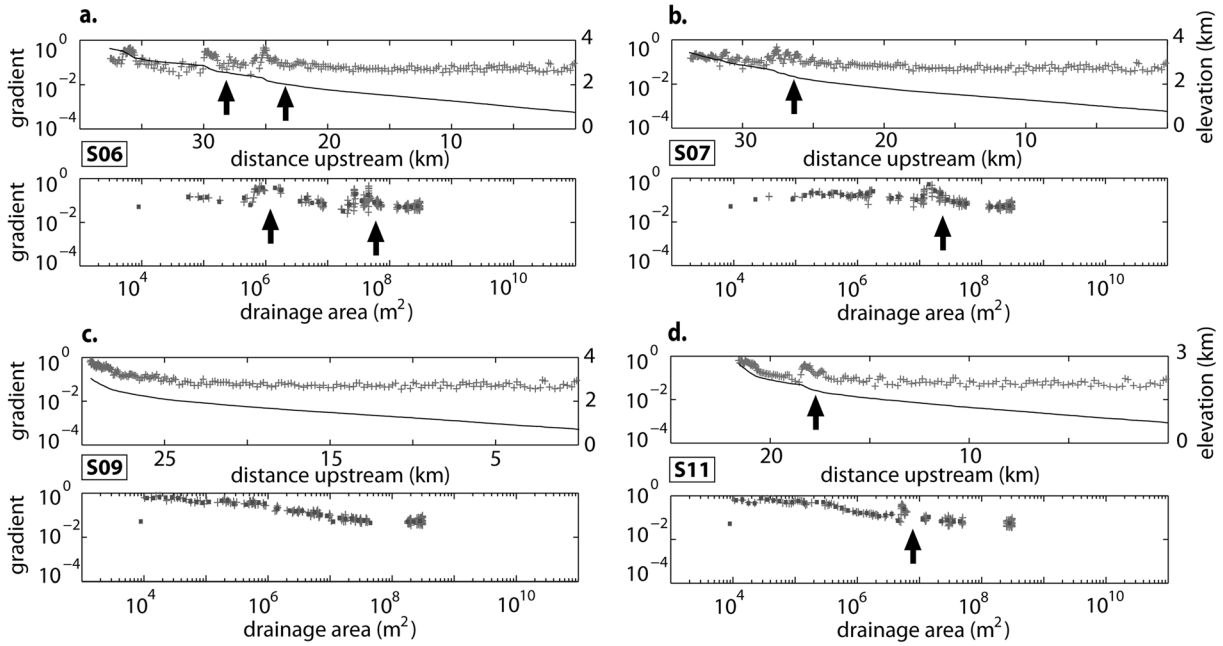

Figure 4. Slope-area plots and longitudinal profiles for each major tributary within Quebrada Veladera: (a) S06, (b) S07, (c) S09, and (d) S11. Crosses and squares represent the channel gradients with different degrees of smoothing. Channel elevations are plotted as lines. Arrows indicate bedrock lithologic boundaries.

an effective elevation, which is the scalar value that reproduces the hypsometrically weighted mean production rate of the sample's upstream drainage area (as suggested by *Balco et al*. [2008]). We omitted low-quartz bedrock areas (such as andesite or gabbro) from the production calculations because they contribute insignificant amounts of quartz to our samples (Figure 1). We did not correct for topographic or snow shielding; topographic shielding is 1.5 to 2.5% at all sampling locations, and the drainage has probably never had perennial snow cover [*Klein et al*., 1999; *Smith et al*., 2005]. Because we observed that the terrace thickness decreased systematically from about 9 to 3 m between our lowest and highest sampling sites, we corrected terrace samples for postdepositional ^{10}Be production by neutron spallation, using a density of 2.0 g/cm^3, an attenuation length of 160 g/cm^2 [*Gosse and Phillips*, 2001], and an approximate terrace age of 16 ka. We ignored production by muons for this correction because they attenuate slowly with depth, imparting a much less systemic error, and because they are responsible for at most a few percent of the total surface cosmogenic production at sea level [*Heisinger et al*., 2002a, 2002b]. The postdepositional production correction changed the erosion rates recorded in the terrace by a maximum of 6.5%. We did not correct terrace samples for the radioactive decay during the time since deposition; the half-life is long enough [*Chmeleff et al*., 2010] that only a tiny fraction of the initial ^{10}Be has decayed since ~16 ka. We used external uncertainties when plotting our results because they are the most conservative estimates of uncertainty [*Balco et al*., 2008].

4. Results

4.1. Modern Stream Profiles

[23] Slope-area plots and longitudinal profiles reveal knickzones in three of the four major tributaries of Quebrada Veladera (Figure 4). In each case, the knickzone is located near the point where the stream channel crosses a bedrock lithologic boundary. The fourth major tributary, upstream from S09, shows no evidence of a knickzone; the bedrock along the channel is uniform granodiorite, supporting the idea that the knickzones were lithologically controlled. No major faults has been mapped in Quebrada Veladera, and it is difficult to connect all three knickzones on a straight line (such as an unmapped fault) or at an elevation contour (suggesting a uniform response to base level change) [*Wobus et al*., 2006].

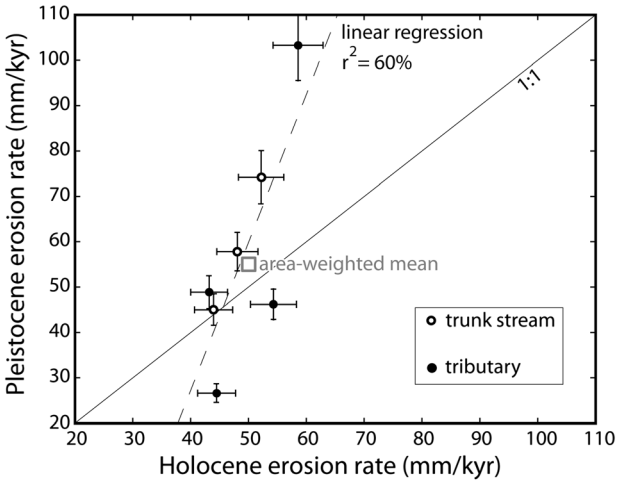

Figure 5. Plot of Holocene and Late Pleistocene erosion rates. Rates were calculated from ^{10}Be concentrations both in modern stream sands collected from the active channel and in sand-size sediment excavated from the base of the Q2 terrace fill.

Table 2. Cosmogenic ^{10}Be Erosion Rates

Site ID	Sample ID	Depth Below Terrace Tread[a] (cm)	Latitude (°)	Longitude (°)	Elevation (m)	Effective Elevation[b] (m)	Drainage Area (km^2)	Contributing Area[c] (km^2)	^{10}Be[d] ($\times 10^5$ atoms g^{-1})	^{10}Be[e] ($\times 10^5$ atoms g^{-1})	Neutron Spallation Production Rate[g,h] (atoms g^{-1} yr^{-1})	Erosion Rate[g] (mm kyr^{-1})	Internal Uncertainty[f,g] (mm kyr^{-1})	External Uncertainty[g,i] (mm kyr^{-1})
S03	QVP-001	-	−13.61606	−75.72112	931	2105	302	140	1.68	-	12.37	54.3	1.1	4.0
S03	QVP-002	900	−13.61606	−75.72112	931	2105	302	140	1.96	1.96	12.37	46.2	0.8	3.4
S06	QVP-007	-	−13.51873	−75.64864	1754	2257	73	12	2.26	-	13.57	43.2	0.7	3.2
S06	QVP-008	230	−13.51873	−75.64864	1754	2257	73	12	2.10	2.01	13.57	48.9	0.8	3.6
S07	QVP-009	-	−13.51237	−75.65296	1767	2323	56	16	2.28	-	14.13	44.5	0.7	3.3
S07	QVP-010	300	−13.51237	−75.65296	1767	2323	56	16	3.77	3.73	14.13	26.6	0.3	2.0
S09	QVP-011	-	−13.52161	−75.67484	1664	2208	39	29	1.64	-	13.17	58.6	1.2	4.3
S09	QVP-012	250	−13.52161	−75.67484	1664	2208	39	29	1.01	0.946	13.17	103.3	2.8	7.8
S10	QVP-014	-	−13.54115	−75.67829	1506	2171	189	73	2.13	-	12.87	44.0	1.0	3.3
S10	QVP-015	250	−13.54115	−75.67829	1506	2171	189	73	2.14	2.08	12.87	45.0	1.1	3.4
S11	QVP-017	-	−13.56724	−75.70559	1295	2151	50	38	1.79	-	12.72	52.2	1.3	3.9
S11	QVP-018	350	−13.56724	−75.70559	1295	2151	50	38	1.28	1.27	12.72	74.2	2.6	5.8
S12	QVP-019	-	−13.57620	−75.70686	1239	2130	256	122	1.91	-	12.56	48.1	1.0	3.6
S12	QVP-020	900	−13.57620	−75.70686	1239	2130	256	122	1.60	1.60	12.56	57.8	1.3	4.3

[a]Not applicable to modern samples, which were collected from active stream sediment.

[b]Effective elevation, which reproduces the hypsometrically weighted drainage-average production rate when entered into Cosmic-Ray Produced Nuclide Systematics (CRONUS), as suggested by *Balco et al.* [2008].

[c]Excludes areas with bedrock containing little or no quartz (Figure 1).

[d]Accelerator mass spectrometer (AMS) results were normalized to the National Institute of Standards and Technology (NIST) standard with a ^{10}Be/^{9}Be ratio of 2.79×10^{-11}. The process-blank ratio averaged $2.84 \times 10^{-16} \pm 7.91 \times 10^{-17}$ for two measurements, amounting to 0.003% to 0.43% of the sample ratios. This ratio was subtracted from sample ratios before conversion to concentration.

[e]Corrected for postdepositional production by neutron spallation using an attenuation length of 160 g cm^{-2} [*Gosse and Phillips*, 2001], a density of 2.0 g cm^{-3}, and an exposure age of 16 ka.

[f]Includes propagated AMS analytical uncertainty and uncertainty in the process-blanks at 1σ.

[g]Calculated using the CRONUS-Earth calculator v. 2.2.1 [*Balco et al.*, 2008] using a constant production rate model and scaling scheme for spallation of *Lal* [1991] and *Stone* [2000]. This version of the CRONUS calculator uses a reference spallogenic sea-level, high-latitude ^{10}Be production rate of 4.49 ± 0.39 atoms g^{-1} yr^{-1} (± 1σ), muonogenic production after *Heisinger et al.* [2002a, 2002b], and standardization factor NIST_27900.

[h]Values at Earth's surface.

[i]The 1σ values propagated from all sources, including AMS analytical, surface production, and scaling uncertainties [*Balco et al.*, 2008].

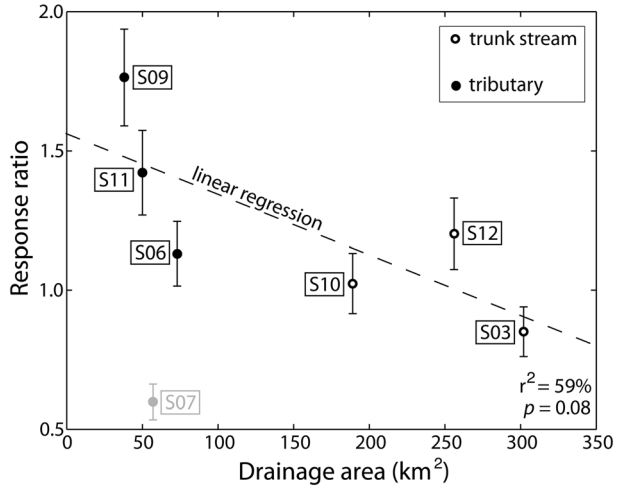

Figure 6. Plot of response ratio and drainage area. The response ratio at each sampling site is equal to the Pleistocene erosion rate divided by the Holocene erosion rate. With the exception of an outlier at S07, response ratio correlates with drainage area. The ^{10}Be erosion rates are calculated from the contributing drainage areas, meaning only the drainage areas containing bedrock with significant quartz content. This plot uses the complete drainage areas because our interest is in landscape dissection. The trend holds regardless of this choice.

[24] The close association of knickzones and bedrock boundaries suggests that the modern channel is not experiencing an ongoing response to climatic or tectonic forcing. Instead, the channel is probably near its graded profile with respect to the local differences in bedrock strength. This interpretation is consistent with Quebrada Veladera's position below the major knickzone on the Pisco River, which is thought to have formed in response to surface uplift at ~10 Ma [*Abbühl et al*., 2011]. As a result, Quebrada Veladera is a relatively blank slate for evaluating climatic forcing on Pleistocene-Holocene timescales.

4.2. Cosmogenic ^{10}Be Erosion Rates

[25] Cosmogenic erosion rates from modern stream sediments are uniform throughout the drainage (Figure 5). Modern sands yield ^{10}Be concentrations between 1.68×10^5 and 2.28×10^5 atoms/g, which correspond to drainage-average erosion rates between 43 ± 3 and 58 ± 4 mm/kyr (Table 2). The mean rate is 49 mm/kyr and the median is 48 mm/kyr. In contrast, erosion rates from Late Pleistocene samples vary by more than a factor of 3. The terrace ^{10}Be concentrations range from 9.46×10^4 to 3.73×10^5 atoms/g, which correspond to paleoerosion rates between 27 ± 2 and 103 ± 8 mm/kyr when postdepositional in situ production has been removed. The mean rate is 57 mm/kyr and the median is 49 mm/kyr. The erosion rates from modern and terrace samples are correlated: Slightly faster erosion rates in the modern samples predict substantially faster rates in the terrace samples (Figure 5).

[26] The ^{10}Be concentrations in the Q2 terrace fill were inherited from ^{10}Be production that took place prior to deposition. Following *Schaller et al*. [2002], we interpret the ^{10}Be concentrations from these deposits as paleoerosion rates. The ^{10}Be-derived erosion rates integrate instantaneous erosion rates over the duration (depth) of ^{10}Be production, weighted toward the most recent rates [e.g., *Bierman and Steig*, 1996]. The integration timescale is set principally by the time that a sample spends moving through a column of hillslope regolith [e.g., *Heimsath et al*., 1997, 1999; *Wittmann and Von Blanckenburg*, 2009]. The *e*-folding timescale for integration is about 12 kyr at an average erosion rate of 50 mm/kyr. Therefore, the terrace samples provide a weighted average of the hillslope erosion rate during the ~12 kyr prior to the deposition of the Q2 fill in the Late Pleistocene. In contrast, the ^{10}Be concentrations in modern sediment reflect erosion rates since ~12 ka, weighted toward the Late Holocene. Although ^{10}Be concentrations provide only minimum estimates of erosion rates during short-lived excursions, the method is sensitive enough to capture Late Pleistocene-Holocene changes (supporting information).

[27] Late Pleistocene erosion rates are as much as 80% higher than the Holocene rates in the tributaries. In contrast, Late Pleistocene and Holocene erosion rates are nearly identical near the outlet of Quebrada Veladera. This contrast reflects a correlation between drainage area and response ratio, which we define as the Late Pleistocene rate divided by the Holocene rate (Figure 6). The tributary upstream from sample S07 is an outlier, a small drainage with a response ratio less than 1. The correlation, including the outlier at S07, is robust and independent of many of our choices in the analysis. For example, the correlation exists regardless of the choice of production scaling model, the exclusion of low-quartz bedrock contributions from production calculations, or the correction for postdepositional ^{10}Be production in the terrace. The outlier is excluded from the regression because its residual is typically outside the 95% confidence interval of the *t* distribution.

[28] Neither the Late Pleistocene nor Holocene erosion rates correlate with average drainage slope, probably because drainage-average slopes in the tributaries and along the trunk of Quebrada Veldera are remarkably similar when calculated using 30 m digital elevation data [*NASA*, 2006]. The mean slope in the contributing area of the quebrada is 23.3°, and the mean basin slope upstream from any sampling point never deviates beyond the range from 22.0° to 25.0°.

4.3. Sediment Storage and Buffering Capacity

[29] The presence of fill terraces in Quebrada Veladera is clear evidence of sediment storage, which has the potential to buffer ^{10}Be concentrations [e.g., *Wittmann et al*., 2011a; *Davis et al*., 2012]. We constrain the potential for buffering in our samples by comparing the volume of sediment stored in the stream channels to the total volume of sediment eroded during the Tauca highstand, when the Q2 terrace formed. The ^{10}Be concentrations provide a measure of the total volume of eroded material. We assume a steady, uniform erosion rate of 55 mm/kyr, which is the area-weighted mean erosion rate derived from the Q2 terrace samples. At this rate, the total volume of material eroded from the quebrada during 14 kyr of the Tauca highstand (25 to 11 ka) was 0.24 km^3. Using a combination of field measurements and aerial imagery, we also calculate the volume of the fill below the Q2 terrace, prior to incision, to be 0.022 km^3. Approximately 10% of the total eroded volume was stored as Q2 terrace fill. This is a maximum value because it does not account for the density contrast between bedrock and fill. The geologic map shows 13 km^2 of Quaternary alluvium in the quebrada, including the Q2 terrace

fill (Figure 1). If this alluvium has an average thickness of 8 m, which is conservatively estimated from observations in the field, then the total volume of sediment in and around the modern channel is approximately 0.104 km^3. Of this, 0.082 km^3 of sediment either predates the Q2 terrace fill or accumulated since its incision. We interpret this volume as a rough estimate of the amount of sediment available for buffering at the time of the Q2 terrace fill deposition. In other words, the total volume of eroded sediment exceeded the volume available for buffering by a factor of 3 or more.

5. Discussion

5.1. Pleistocene-Holocene Landscape Change

[30] In Quebrada Veladera, Late Pleistocene drainage-average erosion rates are similar to corresponding Holocene rates at the points in the channels with larger upstream drainage areas (typically those on the trunk stream). In contrast, Late Pleistocene rates are usually higher than the Holocene rates at the points with smaller upstream areas (typically tributaries) (Figure 6). We interpret the differences to reflect spatial variability in the rate of erosion through time. Although stored sediment may have modestly buffered the apparent trunk stream erosion rates, the amount of sediment stored in the channel is relatively small, and prior work in other locations suggests that only a fraction of stored sediment is available for mixing [*Kelsey and Lamberson*, 1986; *Wittmann and Von Blanckenburg*, 2009; *Wittmann et al*., 2011b]. In addition, stochastic events, such as large landslides, probably do not bias the erosion rates significantly. Even the smallest tributary has an area of 40 km^2. The fluvial character of the terrace deposits and their polymict lithologies suggest that sediment mixing was rapid and thorough. Combined with a modest amount of storage along the channels, these observations suggest that sediment delivered by large landslides is unlikely to control measured ^{10}Be concentrations and the erosion rates derived from them [*Niemi et al*., 2005; *Yanites et al*., 2009].

[31] The negative correlation between response ratio and drainage area suggests that smaller drainage areas are more sensitive to climatic fluctuations than larger ones (Figure 6). In our interpretation, the climate became wetter and possibly stormier at the onset of the Tauca highstand. This change caused channel heads to migrate upslope, eroding hillslopes and forming new channel segments [e.g., *Reneau et al*., 1986; *Montgomery and Dietrich*, 1988; *Rinaldo et al*., 1995; *Tucker and Slingerland*, 1997]. The mechanism for landscape dissection may have been a shift in the threshold for channel formation [e.g., *Montgomery and Dietrich*, 1988]. Smaller drainage areas show higher Late Pleistocene erosion rates than larger ones because smaller tributaries tend to have a higher proportion of first-order channels [*Montgomery and Dietrich*, 1992; *Montgomery and Foufoula-Georgiou*, 1993].

[32] The sudden increase in sediment supply to the channels probably exceeded transport capacity, leading to the deposition of the Q2 terrace fill. Both the composition of the fill and the character of modern landscapes suggest that hillslope erosion occurred in a large part by shallow slumps and debris flows. Many of these flows were mixed into a braided stream network prior to deposition, while some were preserved in place. The overall fining upward of the Q2 fill (Figure 3) suggests that sediment supply eventually waned, driving terrace planation and incision.

[33] The uniform pattern of Holocene erosion rates is consistent with a region of nearly uniform hillslope gradients. With the return to arid conditions following the Tauca highstand, the drainage network likely began annealing by deposition in the channel heads. The spatial uniformity of Holocene erosion rates may reflect a hysteresis in landscape response. Channels are cut relatively quickly when the threshold for channel formation decreases, but infilling of the channel heads may progress slowly after an increase in the threshold [*Montgomery and Dietrich*, 1992].

[34] There is one outlier in our response ratio plot, which is also consistent with drainage network expansion during the Tauca highstand (Figure 6). The bedrock upstream from the outlier at S07 is primarily andesite, shale, and limestone. All three of these lithologies contribute very little quartz to the sediment load, meaning that these areas are not represented by our samples. In fact, the only mapped exposures of quartz-bearing granodiorite and tonalite in S07 are located along the channel near the bottom of the drainage, where channel heads are least likely to occur (Figure 1). A response ratio <1 at S07 is therefore consistent with *less* erosion along the channel—where granitic bedrock was exposed—during the Tauca highstand. This is a plausible response if the drainage network expanded upstream into quartz-poor regolith and then armored the downstream channel with quartz-poor sediment [e.g., *Sklar and Dietrich*, 2001].

[35] We note that both our data and our interpretation are consistent with a frequently applied conceptual model for the formation of fill terraces and alluvial fans. Generally, this model holds that precipitation change destabilizes hillslope sediment that drives aggradation around channels. Eventually, streams plane the valley floors and incise both terraces and fans. There are several possible drivers of hillslope destabilization and subsequent incision, including a decrease in mean annual precipitation [e.g., *Bull*, 1991], an increase in mean annual precipitation [e.g., *Owen et al*., 2006; *Liu and Broecker*, 2008; *DeLong et al*., 2008], and an increase in the number of extreme storm events [e.g., *McDonald et al*., 2003; *Keefer et al*., 2003]. Despite its frequent application, this conceptual model has rarely been tested in the geologic record [*Dorn*, 2009; *Enzel et al*., 2012]. Adequate tests are limited by geologic preservation, the precision of dating methods, and independent constraints on past climate change.

[36] Coupled numerical models [e.g., *Smith and Bretherton*, 1972; *Rinaldo et al*., 1995; *Benda and Dunne*, 1997; *Tucker and Slingerland*, 1997; *Moglen et al*., 1998; *Tucker and Bras*, 1998; *Lague et al*., 2005] and studies of modern landscapes [e.g., *Reneau et al*., 1986; *Montgomery and Dietrich*, 1988, 1992; *van der Beek and Bishop*, 2003; *DiBiase and Whipple*, 2011; *Bookhagen and Strecker*, 2012] have helped to circumvent the limitations of the geologic record. Much of this work supports the hypothesis that climate change drives landscape dissection by exceeding thresholds for sediment transport or channel formation. However, studies of modern landscapes are not necessarily appropriate for understanding landscape responses in the geologic past [e.g., *Aalto et al*., 2006; *Enzel et al*., 2012; *Ferrier et al*., 2013]. Moreover, this work is often restricted to small drainages in humid climates. Arid landscapes have received less attention, prompting comparisons between models and landscapes in substantially different settings

[e.g., *Steffen et al*., 2009]. *Reneau et al*. [1986] use ^{14}C dating to show that 11 colluvial hollows in California have filled only since the Late Pleistocene, indicating that colluvium was flushed from the system around the Pleistocene-Holocene transition. With the exception of this work, our study presents the first direct evidence of landscape dissection following a change in precipitation over geologic timescales.

5.2. Regional Comparison and Implications for Climate

[37] Many studies have examined the formation of alluvial fans and terraces in the Altiplano and the Western Cordillera beyond the Pisco River [*Steffen et al*., 2009]. The regional coincidence of paleolake highstands with alluvial fan and terrace formation suggests that increased precipitation drives sediment from hillslopes into channels. *Steffen et al*. [2010] link periods of deposition along the Majes River, south of the Pisco, to a highstand from 98 to 120 ka, the Minchin highstand, and the Tauca (specifically, the Coipasa) highstand. *Rigsby et al*. [2003] and *Farabaugh and Rigsby* [2005] link aggradation events on the Altiplano to the Minchin and Tauca highstands, as well as to Holocene lake levels changes. Clusters of landslide deposits in the northern Argentine Andes were deposited during the Minchin highstand and a Late Holocene highstand [*Trauth et al*., 2003]. Although not all wet intervals are reported at each site, the regional pattern shows deposition to be synchronous with wet intervals. The complex response of landscapes to local differences in environmental variables, such as weathering rate, may explain the regional discrepancies in the depositional record [*Schumm*, 1973].

[38] Our interpretation favors a precipitation change in the Late Pleistocene that shifted the threshold for channel formation on the hillslopes. The frequency of extreme precipitation events, or storminess, is often associated with threshold changes [e.g., *Reneau et al*., 1986; *Tucker and Slingerland*, 1997; *Harvey et al*., 1999; *McDonald et al*., 2003; *Molnar et al*., 2006]. ENSO is an appealing explanation for past changes in storminess because historic El Niño events have been shown to cause erosion and sediment transport on a large scale [*Keefer et al*., 2003; *Mettier et al*., 2009; *Abbühl et al*., 2010]. Near the Peruvian coast, Quaternary depositional events are often attributed to changes in the state of ENSO [*Sandweiss et al*., 2001; *Keefer et al*., 2003; *Ortlieb and Vargas*, 2003; *Sandweiss*, 2003]. These attributions are most common in the Holocene, when records show the onset of modern ENSO periodicity [*Rodbell et al*., 1999; *Moy et al*., 2002], but several studies have pushed this interpretation back into the Late Pleistocene [*Keefer et al*., 2003; *Rein*, 2005; *Makou et al*., 2010].

[39] Despite evidence for changes in ENSO, we agree with the interpretation of *Steffen et al*. [2009] and discount the role of ENSO in the formation of the terraces of Quebrada Veladera and the Pisco River. IRSL dates clearly link the deposition of terraces T1 and T2 on the Pisco River (and therefore Q1 and Q2 in Quebrada Veladera) to the Minchin and Tauca paleolake highstands (Table 1). There is evidence for a change in ENSO behavior just after 12 ka, which overlaps with the Tauca highstand [*Keefer et al*., 2003; *Makou et al*., 2010]. However, this change was probably too late to effect the T2 terrace, which has depositional ages from 24 to 16 ka [*Steffen et al*., 2009]. Furthermore, although records indicate that El Niño events have been particularly strong since 5 ka [*Rodbell et al*., 1999; *Keefer et al*., 2003; *Moy et al*., 2002; *Makou et al*., 2010], there is scant evidence for associated hillslope erosion, either as terrace deposition in the Pisco or Quebrada Veladera or as accelerated erosion rates in Quebrada Veladera. Finally, the terraces along the Pisco River begin about 80 km from the coast, at an elevation of almost 3 km. This position is deeper into the mountain front than El Niño events that typically penetrate [*Mettier et al*., 2009; *Abbühl et al*., 2010], even in the north, where their modern effects are strongest [*Lagos et al*., 2008]. The position of the Pisco terraces seems more likely to reflect changes in upland precipitation, consistent with enhanced easterly winds [*Steffen et al*., 2009, 2010]. Because of the close association of the Pisco and Quebrada Veladera terraces, it seems likely that this precipitation reached as far west as Quebrada Veladera.

[40] Although we minimize the role of ENSO, changes in storminess could be important. Perhaps the climate was both wetter and stormier during the Tauca highstand. However, the proportion of precipitation delivered by extreme storm events is usually lower in wetter climates than in drier ones [*Turcotte and Greene*, 1993; *Molnar et al*., 2006]. *Molnar et al*. [2006] note that in extremely arid regions, where almost no precipitation reaches the ground, any increase in the amount of precipitation will tend to drive stream incision. It is possible that additional precipitation, delivered in many moderately sized events, may have driven landscape dissection in Quebrada Veladera.

6. Conclusions

[41] In Quebrada Veladera, paired sampling allows for comparison of the ^{10}Be erosion rates recorded by modern sediments with the paleoerosion rates recorded by quartz in terrace sediments, which were deposited just after the Last Glacial Maximum. The climate was substantially wetter at that time, but Quebrada Veladera was probably never glaciated [*Klein et al*., 1999; *Smith et al*., 2005]. As a result, the comparison tests the response of a landscape shaped by stream and hillslope processes to precipitation change. Downstream, near the mouth of the quebrada, Late Pleistocene and Holocene erosion rates are similar. However, smaller, upstream tributaries record up to 80% faster erosion in the Late Pleistocene. The spatially variable erosion response, characterized by stronger responses in smaller tributaries, suggests that the drainage network expanded upslope during the Tauca paleolake highstand, when the climate was wetter, tapping into sediment stored on the hillslopes. With a return to arid conditions, the drainage network gradually annealed. The climate may have been stormier, as well as wetter, during the Tauca highstand, but the timing and extent of terrace formation does not suggest that ENSO variability had an important role. Unlike other interpretations of the geologic record, ours provides direct evidence for landscape dissection and annealing in response to climate change. This result supports widely used conceptual models [e.g., *Tucker and Slingerland*, 1997; *Dorn*, 2009] and implies that smaller drainage areas are more sensitive to climate changes than larger ones.

[42] **Acknowledgments.** Constructive comments from Associate Editor Nicole Gasparini and three anonymous reviewers improved this manuscript. The work was supported by National Science Foundation grant EAR-1049300 (DM).

References

Aalto, R., T. Dunne, and J. L. Guyot (2006), Geomorphic controls on Andean denudation rates, *J. Geol.*, *114*(1), 85–99.

Abbühl, L. M., K. P. Norton, F. Schlunegger, O. Kracht, A. Aldahan, and G. Possnert (2010), El Niño forcing on ^{10}Be-based surface denudation rates in the northwestern Peruvian Andes?, *Geomorphology*, *123*, 257–268.

Abbühl, L. M., K. P. Norton, J. D. Jansen, F. Schlunegger, A. Aldahan, and G. Possnert (2011), Erosion rates and mechanisms of knickzone retreat inferred from ^{10}Be measured across strong climate gradients on the northern and central Andes Western Escarpment, *Earth Surf. Processes Landforms*, *36*(11), 1464–1473.

Agteca (2010), Global Historical Climatology Network (GHCN monthly database) compilation for Peru by T.A. Cochrane. Downloaded January 2012 from Agteca.org.

Anders, M. D., J. L. Pederson, T. M. Rittenour, W. D. Sharp, J. C. Gosse, K. E. Karlstrom, L. J. Crossey, R. J. Goble, L. Stockli, and G. Yang (2005), Pleistocene geomorphology and geochronology of the eastern Grand Canyon: Linkages of landscape components during climate changes, *Quat. Sci. Rev.*, *24*, 2428–2448.

Baker, P. A., C. A. Rigsby, G. O. Seltzer, S. C. Fritz, T. K. Lowenstein, N. P. Bacher, and C. Veliz (2001a), Tropical climate changes at millennial and orbital timescales on the Bolivian Altiplano, *Nature*, *409*(6821), 698–701.

Baker, P. A., G. O. Seltzer, S. C. Fritz, R. B. Dunbar, M. J. Grove, P. M. Tapia, S. L. Cross, H. D. Rowe, and J. P. Broda (2001b), The history of South American tropical precipitation for the past 25,000 years, *Science*, *291*(5504), 640–643.

Balco, G., J. O. Stone, N. A. Lifton, and T. J. Dunai (2008), A complete and easily accessible means of calculating surface exposure ages or erosion rates from< ^{10}Be and ^{26}Al measurements, *Quat. Geochronol.*, *3*(3), 174–195.

Benda, L., and T. Dunne (1997), Stochastic forcing of sediment routing and storage in channel networks, *Water Resour. Res.*, *33*(12), 2865–2880.

Bierman, P. R., and K. K. Nichols (2004), Rock to sediment-slope to sea with 10Be-rates of landscape change, *Annu. Rev. Earth Planet. Sci.*, *32*, 215–255.

Bierman, P., and E. J. Steig (1996), Estimating rates of denudation using cosmogenic isotope abundances in sediment, *Earth Surf. Processes Landforms*, *21*(2), 125–139.

Bookhagen, B., and M. R. Strecker (2012), Spatiotemporal trends in erosion rates across a pronounced rainfall gradient: Examples from the southern Central Andes, *Earth Planet. Sci. Lett.*, *327*, 97–110.

Brown, E. T., R. F. Stallard, M. C. Larsen, G. M. Raisbeck, and F. Yiou (1995), Denudation rates determined from the accumulation of in situ-produced ^{10}Be in the Luquillo experimental forest, Puerto Rico, *Earth Planet. Sci. Lett.*, *129*(1), 193–202.

Bull, W. B. (1991), *Geomorphic Responses to Climate Change*, pp. 326, Oxford Univ. Press, Oxford.

Chmeleff, J., F. von Blanckenburg, K. Kossert, and D. Jakob (2010), Determination of the ^{10}Be half-life by multicollector ICP-MS and liquid scintillation counting, *Nucl. Instrum. Methods Phys. Res., Sect. B: Beam Interactions With Materials and Atoms*, *268*(2), 192–199.

Corbett, L. B., N. E. Young, P. R. Bierman, J. P. Briner, T. A. Neumann, D. H. Rood, and J. A. Graly (2011), Paired bedrock and boulder ^{10}Be concentrations resulting from early Holocene ice retreat near Jakobshavn Isfjord, western Greenland, *Quat. Sci. Rev.*, *30*(13), 1739–1749.

Costa, J. E. (1988), Rheologic, geomorphic, and sedimentologic differentiation of water floods, hyperconcentrated flows, and debris flows, in *Flood Geomorphology*, edited by V. R. Baker, R. C. Rochel, and P. C. Patton, pp. 113–122, Wiley, New York.

Cox, R., P. Bierman, M. C. Jungers, and A. F. M. Rakotondrazafy (2009), Erosion rates and sediment sources in Madagascar inferred from ^{10}Be analysis of Lavaka, slope, and river sediment, *J. Geol.*, *117*(4), 363–376.

Davila, M. F. (1979), Mapa Geologico del Cuadrangula de Guadalupe, *1:100,000*, Ministerio de Energia y Minas, Peru.

Davis, M., A. Matmon, D. H. Rood, and S. Avnaim-Katav (2012), Constant cosmogenic nuclide concentrations in sand supplied from the Nile River over the past 2.5 m.y, *Geology*, *40*(4), 359–362.

DeLong, S. B., J. D. Pelletier, and L. J. Arnold (2008), Climate change triggered sedimentation and progressive tectonic uplift in a coupled piedmont-axial system: Cuyama Valley, California, USA, *Earth Surf. Processes Landforms*, *33*, 1033–1046.

Diaz, H. S., and C. Landa (1970), Mapa Geologicao del Cuadrangula de Tantara, Ministerio de Energia y Minas, Peru.

DiBiase, R. A., and K. X. Whipple (2011), The influence of erosion thresholds and runoff variability on the relationships among topography, climate, and erosion rate, *J. Geophys. Res.*, *116*, F04036, doi:10.1029/2011JF002095.

Dorn, R. I. (2009), The role of climate change in alluvial fan development, in *Geomorphology of Desert Environments*, edited by A. J. Parsons and A. D. Abrahams, pp. 593–615, Springer, Netherlands.

Enzel, Y., R. Amit, T. Grodek, A. Ayalon, J. Lekach, N. Porat, P. Bierman, J. D. Blum, and Y. Erel (2012), Late Quaternary weathering, erosion, and deposition in Nahal Yael, Israel: An "impact of climatic change on an arid watershed"?, *Geol. Soc. Am. Bull.*, *124*(5–6), 705–722.

Farabaugh, R. L., and C. A. Rigsby (2005), Climatic influence on sedimentology and geomorphology of the rio ramosvalley, Peru, *J. Sediment. Res*, *75*, 12–28.

Ferrier, K. L., K. L. Huppert, and J. T. Perron (2013), Climatic control of bedrock river incision, *Nature*, *496*, 206–209.

Fritz, S. C., P. A. Baker, T. K. Lowenstein, G. O. Seltzer, C. A. Rigsby, G. S. Dwyer, P. M. Tapia, K. K. Arnold, T.-L. Ku, and S. Luo (2004), Hydrologic variation during the last 170,000 years in the southern hemisphere tropics of South America, *Quat. Res.*, *61*(1), 95–104.

Fuller, T. K., L. A. Perg, J. K. Willenbring, and K. Lepper (2009), Field evidence for climate-driven changes in sediment supply leading to strath terrace formation, *Geology*, *37*(5), 467–470.

Garreaud, R., M. Vuille, and A. C. Clement (2003), The climate of the Altiplano: Observed current conditions and mechanisms of past changes, *Palaeogeogr. Palaeoclimatol. Palaeoecol.*, *194*(1), 5–22.

Garreaud, R. D., M. Vuille, R. Compagnucci, and J. Marengo (2009), Present-day South American climate, *Palaeogeogr. Palaeoclimatol. Palaeoecol.*, *281*(3), 180–195.

Gosse, J. C., and F. M. Phillips (2001), Terrestrial in situ cosmogenic nuclides: Theory and application, *Quat. Sci. Rev.*, *20*(14), 1475–1560.

Graf, W. L. (1987), Late Holocene sediment storage in canyons of the Colorado Plateau, *Geol. Soc. Am. Bull.*, *99*(2), 261–271.

Granger, D. E., J. W. Kirchner, and R. Finkel (1996), Spatially averaged long-term erosion rates measured from in situ-produced cosmogenic nuclides in alluvial sediment, *J. Geol.*, *104*, 249–257.

Harvey, J. E. (2005), Looking at the Grand Canyon—and finding some answers!, *Quat. Sci. Rev.*, *24*, 2426–2427.

Harvey, J. E., and J. L. Pederson (2011), Reconciling arroyo cycle and paleoflood approaches to late Holocene alluvial records in dryland streams, *Quat. Sci. Rev.*, *30*(7), 855–866.

Harvey, J. E., P. E. Wigand, and S. G. Wells (1999), Response of alluvial fan systems to the late Pleistocene to Holocene climatic transition: Contrasts between the margins of pluvial Lake Lahontan and Mojave, Nevada and California, USA, *Catena*, *36*, 255–281.

Heimsath, A. M., W. E. Dietrich, K. Nishiizumi, and R. C. Finkel (1997), The soil production function and landscape equilibrium, *Nature*, *388*(6640), 358–361.

Heimsath, A. M., W. E. Dietrich, K. Nishiizumi, and R. C. Finkel (1999), Cosmogenic nuclides, topography, and the spatial variation of soil depth, *Geomorphology*, *27*(1), 151–172.

Heisinger, B., D. Lal, A. Jull, P. Kubik, S. Ivy-Ochs, K. Knie, and E. Nolte (2002a), Production of selected cosmogenic radionuclides by muons: 2. Capture of negative muons, *Earth Planet. Sci. Lett.*, *200*(3), 357–369.

Heisinger, B., D. Lal, A. Jull, P. Kubik, S. Ivy-Ochs, S. Neumaier, K. Knie, V. Lazarev, and E. Nolte (2002b), Production of selected cosmogenic radionuclides by muons: 1 Fast muons, *Earth Planet. Sci. Lett.*, *200*(3), 345–355.

Keefer, D. K., E. M. Moseley, and S. D. de France (2003), A 38,000-year record of floods and debris flows in the Ilo region of southern Peru and its relation to El Niño events and great earthquakes, *Palaeogeogr. Palaeoclimatol. Palaeoecol.*, *194*, 41–77.

Kelsey, H., and R. Lamberson (1986), Modeling the transport of stored sediment in a gravel bed river, northwestern California, *IAHS-AISH Publ.*, *159*, 367–391.

Klein, A. G., G. O. Seltzer, and B. L. Isacks (1999), Modern and last local glacial maximum snowlines in the Central Andes of Peru, Bolivia, and Northern Chile, *Quat. Sci. Rev.*, *18*(1), 63–84.

Kohl, C. P., and K. Nishiizumi (1992), Chemical isolation of quartz for measurement of in-situ produced cosmogenic nuclides, *Geochim. Cosmica. Acta.*, *56*, 3583–3587.

Lagos, P., Y. Silva, E. Nickl, and K. Mosquera (2008), El Niño-related precipitation variability in Perú, *Adv.Geosci.*, *14*, 231–237.

Lague, D., N. Hovius, and P. Davy (2005), Discharge, discharge variability, and the bedrock channel profile, *J. Geophys. Res.*, *110*, F04006, doi:10.1029/2004JF000259.

Lal, D. (1991), Cosmic ray labeling of erosion surfaces: In situ nuclide production rates and erosion models, *Earth Planet. Sci. Lett.*, *104*(2), 424–439.

Liu, T., and W. S. Broecker (2008), Rock varnish microlamination dating of late Qauternary geomorphic features in the drylands of western USA, *Geomorphology*, *93*, 501–523.

Makou, M. C., T. I. Eglinton, D. W. Oppo, and K. A. Hughen (2010), Postglacial changes in El Niño and La Niña behavior, *Geology*, *38*(1), 43–46.

McDonald, E. V., L. D. McFadden, and S. G. Wells (2003), Regional response of alluvial fans to the Pleistocene-Holocene climatic transition, Mojave Desert, California, *Geol. Soc. Am. Spec. Pap.*, *368*, 189–205.

Mettier, R., F. Schlunegger, H. Schneider, D. Rieke-Zapp, and M. Schwab (2009), Relationships between landscape morphology, climate and surface erosion in northern Peru at 5°S latitude, *Int. J. Earth Sci.*, *98*(8), 2009–2022.

Miall, A. D. (1996), *The Geology of Fluvial Deposits*, pp. 582, Springer, Berlin.

Moglen, G. E., E. A. B. Eltahir, and R. L. Bras (1998), On the sensitivity of drainage density to climate change, *Water Resour. Res.*, *34*(4), 855–862.

Molnar, P., R. S. Anderson, G. Kier, and J. Rose (2006), Relationships among probability distributions of stream discharges in floods, climate, bed load transport, and river incision, *J. Geophys. Res.*, *111*, F02001, doi:10.1029/2005JF000310.

Montgomery, D. R., and W. E. Dietrich (1988), Where do channels begin?, *Nature*, *336*, 232–234.

Montgomery, D. R., and W. E. Dietrich (1992), Channel initiation and the problem of landscape scale, *Science*, *255*(5046), 826–830.

Montgomery, D. R., and E. Foufoula-Georgiou (1993), Channel network source representation using digital elevation models, *Water Resour. Res.*, *29*(12), 3925–3934.

Moy, C. M., G. O. Seltzer, D. T. Rodbell, and D. M. Anderson (2002), Variability of El Niño/Southern Oscillation activity at millenial timescales during the Holocene epoch, *Nature*, *14*, 162–165.

National Aeronautics and Space Administration (NASA) (2006), AST14DEM, USGS/Earth Resources Observation and Science (EROS) Center, Sioux Falls, South Dakota.

National Research Council (2010), *Landscapes on the Edge: New Horizons for Research on Earth's Surface*, pp. 180, The National Academies Press, Washington, D.C.

Niemi, N. A., M. Oskin, D. W. Burbank, A. M. Heimsath, and E. J. Gabet (2005), Effects of bedrock landslides on cosmogenically determined erosion rates, *Earth Planet. Sci. Lett.*, *237*, 480–498.

Nishiizumi, K., M. Imamura, M. W. Caffee, J. R. Southon, R. C. Finkel, and J. McAninch (2007), Absolute calibration of ^{10}Be AMS standards, *Nucl. Instrum. Methods Phys. Res., Sect. B: Beam Interactions With Materials and Atoms*, *258*(2), 403–413.

Ortlieb, L., and G. Vargas (2003), Debris-flow deposits and El Niño impacts along the hyperarid southern Peru coast, in *El Niño in Peru: Biology and Culture of 10,000 Years*, edited by J. Haas and M. O. Dillon, pp. 24–51, Field Museum of Natural History, Chicago.

Owen, L. A., R. C. Finkel, M. Haizhou, and P. L. Barnard (2006), Late Quaternary landscape evolution in the Kunlun Mountains and Qaidam Basin, Northern Tibet: A framework for examining the link between glaciation, lake level changes, and alluvial fan formation, *Quat. Int.*, *154–155*, 73–86.

Placzek, C., J. Quade, and P. J. Patchett (2006), Geochronology and stratigraphy of late Pleistocene lake cycles on the southern Bolivian Altiplano: implications for causes of tropical climate change, *Geol. Soc. Am. Bull.*, *118*(5–6), 515–532.

Ramage, J. M., J. A. Smith, D. T. Rodbell, and G. O. Seltzer (2005), Comparing reconstructed Pleistocene equilibrium-line altitudes in the tropical Andes of central Peru, *J. Quat. Sci.*, *20*(7–8), 777–788.

Rein, B., A. Luckge, L. Reinhart, F. Sirocko, A. Wolf, and W.-C. Dullo (2005), El Nino variability off Peru during the last 20,000 years, *Paleoceanography*, *20*, PA4003, doi:10.1029/2004PA001099.

Reneau, S. L., W. E. Dietrich, R. I. Dorn, C. R. Berger, and M. Rubin (1986), Geomorphic and paleoclimatic implications of latest Pleistocene radiocarbon dates from colluvium-mantled hollows, California, *Geology*, *14*(8), 655–658.

Rigsby, C. A., P. A. Baker, and M. S. Aldenderfer (2003), Fluvial history of the Rio Ilave valley, Peru, and its relationship to climate and human history, *Palaeogeogr. Palaeoclimatol. Palaeoecol.*, *194*(1), 165–185.

Rinaldo, A., W. E. Dietrich, R. Rigon, G. K. Vogel, and I. Rodriguez-Iturbe (1995), Geomorphological signatures of varying climate, *Nature*, *374*, 632–635.

Rodbell, D. T. (1992), Late Pleistocene equilibrium-line reconstructions in the northern Peruvian Andes, *Boreas*, *21*(1), 43–52.

Rodbell, D. T., G. O. Seltzer, D. M. Anderson, M. B. Abbott, D. B. Enfield, and J. H. Newman (1999), An ~15,000-year record of El Nino-driven alluviation Southwestern Ecuador, *Science*, *283*, 516–520.

Rollins, H. B., J. B. Richardson, and D. H. Sandweiss (1986), The birth of El Niño: Geoarchaeological evidence and implications, *Geoarchaeology*, *1*(1), 3–15.

Sandweiss, D. H. (2003), Terminal Pleistocene through Mid-Holocene archaeological sites as paleoclimatic archives for the Peruvian coast, *Palaeogeogr. Palaeoclimatol. Palaeoecol.*, *194*, 23–40.

Sandweiss, D. H., K. A. Maasch, R. L. Burger, J. B. Richardson III, H. B. Rollins, and A. Clement (2001), Variation in Holocene El Niño frequencies: Climate records and cultural consequences in ancient Peru, *Geology*, *29*, 603–606.

Schaller, M., and T. Ehlers (2006), Limits to quantifying climate driven changes in denudation rates with cosmogenic radionuclides, *Earth Planet. Sci. Lett.*, *248*(1), 153–167.

Schaller, M., F. Von Blanckenburg, A. Veldkamp, L. Tebbens, N. Hovius, and P. Kubik (2002), A 30 000 yr record of erosion rates from cosmogenic ^{10}Be in middle European river terraces, *Earth Planet. Sci. Lett.*, *204*(1), 307–320.

Schumm, S. A. (1973), Geomorphic thresholds and complex response of drainage systems, in *Fluvial Geomorphology*, edited by M. Morisawa, pp. 299–310, State University of New York, Binghamton.

Sklar, L. S., and W. E. Dietrich (2001), Sediment and rock strength controls on river incision into bedrock, *Geology*, *29*(12), 1087–1090.

Smith, T. R., and F. P. Bretherton (1972), Stability and the conservation of mass in drainage basin evolution, *Water Resour. Res.*, *8*(6), 1506–1529.

Smith, J. A., G. O. Seltzer, D. L. Farber, D. T. Rodbell, and R. C. Finkel (2005), Early local last glacial maximum in the tropical Andes, *Science*, *308*(5722), 678–681.

Steffen, D., F. Schlunegger, and F. Preusser (2009), Drainage basin response to climate change in the Pisco valley, Peru, *Geology*, *37*(6), 491–494.

Steffen, D., F. Schlunegger, and F. Preusser (2010), Late Pleistocene fans and terraces in the Majes valley, southern Peru, and their relation to climatic variations, *Int. J. Earth Sci.*, *99*(8), 1975–1989.

Stone, J. O. (2000), Air pressure and cosmogenic isotope production, *J. Geophys. Res.*, *105*(B10), 23,753–23,759.

Thompson, L. G., M. E. Davis, E. Mosley-Thompson, T. Sowers, K. A. Henderson, V. S. Zagorodnov, P.-N. Lin, V. N. Mikhalenko, R. K. Campen, and J. F. Bolzan (1998), A 25,000-year tropical climate history from Bolivian ice cores, *Science*, *282*(5395), 1858–1864.

Thompson, L. G., E. Mosley-Thompson, M. E. Davis, P.-N. Lin, K. Henderson, and T. A. Mashiotta (2003), Tropical glacier and ice core evidence of climate change on annual to millennial time scales, in *Climate Variability and Change in High Elevation Regions: Past, Present & Future*, edited by H. F. Diaz, pp. 137–155, Springer, Netherlands.

Trauth, M. H., B. Bookhagen, N. Marwan, and M. R. Strecker (2003), Multiple landslide clusters record Quaternary climate changes in the northwestern Argentine Andes, *Paleoceanography*, *194*(1-3), 109–121, doi:10.1016/S0031-0182(03)00273-6.

Tucker, G. E., and R. L. Bras (1998), Hillslope processes, drainage density, and landscape morphology, *Water Resour. Res.*, *34*(10), 2751–2764.

Tucker, G. E., and R. Slingerland (1997), Drainage basin responses to climate change, *Water Resour. Res.*, *33*(8), 2031–2047.

Turcotte, D. L., and L. Greene (1993), A scale-invariant approach to flood-frequency analysis, *Stochastic Hydrol. Hydraul.*, *7*(1), 33–40.

van der Beek, P., and P. Bishop (2003), Cenozoic river profile development in the Upper Lachlan catchment (SE Australia) as a test of quantitative fluvial incision models, *J. Geophys. Res.*, *108*(B6), 2309, doi:10.1029/2002JB002125.

Vargas, G., J. Rutllant, and L. Ortlieb (2006), ENSO tropical-extratropical climate teleconnections and mechanisms for Holocene debris flows along the hyperarid coast of western South America (17 -24S), *EPSL*, *249*, 467–483.

Von Blanckenburg, F. (2005), The control mechanisms of erosion and weathering at basin scale from cosmogenic nuclides in river sediment, *Earth Planet. Sci. Lett.*, *237*(3), 462–479.

Wang, X., A. S. Auler, R. L. Edwards, H. Cheng, P. S. Cristalli, P. L. Smart, D. A. Richards, and C. C. Shen (2004), Wet periods in northeastern Brazil over the past 210 kyr linked to distant climate anomalies, *Nature*, *432*(7018), 740–743.

Wittmann, H., and F. Von Blanckenburg (2009), Cosmogenic nuclide budgeting of floodplain sediment transfer, *Geomorphology*, *109*(3), 246–256.

Wittmann, H., F. von Blanckenburg, L. Maurice, J. L. Guyot, N. Filizola, and P. W. Kubik (2011a), Sediment production and delivery in the Amazon River basin quantified by in situ-produced cosmogenic nuclides and recent river loads, *Geol. Soc. Am. Bull.*, *123*(5–6), 934–950.

Wittmann, H., F. von Blanckenburg, L. Maurice, J. L. Guyot, and P. Kubik (2011b), Recycling of Amazon floodplain sediment quantified by cosmogenic ^{26}Al and ^{10}Be, *Geology*, *39*(5), 467–470.

Wobus, C., K. X. Whipple, E. Kirby, N. Snyder, J. Johnson, K. Spyropolou, B. Crosby, and D. Sheehan (2006), Tectonics from topography: Procedures, promise, and pitfalls, *Spec. Pap. Geol. Soc. Am.*, *398*, 55.

Xu, S., A. B. Dougans, S. P. Freeman, C. Schnabel, and K. M. Wilcken (2010), Improved ^{10}Be and ^{26}Al-AMS with a 5MV spectrometer, *Nucl. Instrum. Methods Phys. Res., Sect. B: Beam Interactions With Materials and Atoms*, *268*(7), 736–738.

Yanites, B. J., G. E. Tucker, and R. S. Anderson (2009), Numerical and analytical models of cosmogenic radionuclide dynamics in landslide-dominated drainage basins, *J. Geophys. Res.*, *114*, F01007, doi:10.1029/2008JF001088.